Journal of Power Sources 195 (2010) 6811–6816

Contents lists available at ScienceDirect

Journal of Power Sources

journal homepage: www.elsevier.com/locate/jpowsour

Bubble assisted synthesis of Sn–Sb–Cu alloy hollow nanostructures and their improved lithium storage properties

Rong Yang[a], Jing Huang[a], Wei Zhao[a], Wenzhong Lai[a,c], Xuanzhou Zhang[a], Jie Zheng[a], Xingguo Li[a,b,*]

[a] Beijing National Laboratory for Molecular Sciences (BNLMS), The State Key Laboratory of Rare Earth Materials Chemistry and Applications, College of Chemistry and Molecular Engineering, Peking University, Beijing 100871, China
[b] College of Engineering, Peking University, Beijing 100871, China
[c] Department of Chemistry and Biology Engineering, Sanming University, Fujian 365004, China

ARTICLE INFO

Article history:
Received 24 February 2010
Received in revised form 16 April 2010
Accepted 21 April 2010
Available online 28 April 2010

Keywords:
Alloy composites
Hollow nanospheres
Anode materials
Lithium-ion batteries

ABSTRACT

Hollow nanospheres of Sn–Sb–Cu alloy composites have been successfully synthesized via co-reduction of metal chlorides in aqueous alkaline solution without using any surfactants or solid templates. A bubble assisted growth mechanism is proposed to account for the formation of the hollow nanostructures. The concentration of the reactants kinetically controls the nucleation rate of the alloy nuclei, making for the formation of the hollow nanospheres. Compared with the alloy nanoparticles, the hollow spheres exhibit relatively high electrochemical capacity and good cyclic retention when used as anode materials for lithium-ion batteries. The bubble assisted synthesis method can be readily explored for fabricating hollow nanostructure of other alloy system for functional material applications.

1. Introduction

Recently, the effort of synthesis of diverse hollow nanospheres has intensively increased due to their intriguing properties, such as low density and economical use of materials, and this has resulted in their potential applications including drug delivery, optical device, catalysis, chemical sensor, lithographic patterning and biotechnology [1–6]. The general approach for preparing hollow metal spheres is using various removable or sacrificial templates such as polymer spheres [1], silica sol [2], reducing metal nanoparticles [3] and even emulsion droplet [4]. However, most of the methods using template synthesis are high cost, time-consuming and extremely complicated. The synthesis methods for most of the templates are complicated, and it is often difficult to maintain the hollow structure during template removal. Consequently, it is preferable to use a facile one-step method to prepare the hollow nanostructures [7–9]. The in situ bubble assisted synthesis method is a convenient approach for the preparation of hollow metal spheres [10–11]. As the hollow nanospheres are fabricated without any solid templates and surfactants, the bubble assisted method is a suitable approach for the fabrication of hollow structures in large-scale applications.

Since Fujiphoto Film Celltec reported that some tin-based oxides exhibited high capacity and stable cycling performance, metal-based anode materials of lithium batteries have attracted much research attention in pursuing higher power density and longer lifetime [12]. In order to overcome the irreversible capacity caused by the formation of Li_2O during electrochemical reaction in the first cycle, intermetallic compounds instead of oxides have been taken into account [13–15]. Owning to their superior lithium storage capacities, metals such as Sn, Sb, Al, Si, and Ag can be good substitutes for the traditional carbon-based anode materials [16]. However, these materials suffer from severe volume change during Li insertion and extraction that often causes electrode disintegration and rapid capacity fading [17,18]. In recent years, considerable effort has been made to overcome this problem by using composite materials [19–25], including Sn–Co [19–22], Sn–Cu [23] and Sn–Ni [24,25] composites. The inactive phase serves as a buffer which partly alleviates mechanical stress caused by the volume change of the active phase. Another promising approach is to fabricate particular nanostructure, because some early researches have proved that the electrochemical performances of the anode materials seem to have strong correlation to the structure features. Such structural modifications might allow us to reduce the initial irreversible capacity and improve the cyclic retention of the nanomaterials.

Here, we used a facile synthesis method for the fabrication of Sn–Sb–Cu hollow nanospheres. The synthesis was performed in

* Corresponding author at: Beijing National Laboratory for Molecular Sciences (BNLMS), The State Key Laboratory of Rare Earth Materials Chemistry and Applications, College of Chemistry and Molecular Engineering, Peking University, Beijing 100871, China. Tel.: +86 10 62765930; fax: +86 10 62765930.
E-mail address: xgli@pku.edu.cn (X. Li).

0378-7753/$ – see front matter © 2010 Elsevier B.V. All rights reserved.
doi:10.1016/j.jpowsour.2010.04.069

aqueous solution by using $NaBH_4$ to co-reduce the metal chlorides. In this reaction, H_2 bubbles generated in situ in the alkali solution under magnetic stirring played a significant role for the formation of the hollow spheres. The bubble assisted synthesis method can also be used for fabricating hollow nanostructure of other alloy system. When used as anode materials for lithium-ion batteries, the Sn–Sb–Cu hollow nanospheres exhibited relatively high electrochemical capacity and good cyclic retention, which could all be attributed to their specific hollow structure.

2. Experimental

Tin dichloride dihydrate ($SnCl_2{\cdot}2H_2O$, >98%), antimony trichloride ($SbCl_3$, >97%), copper dichloride dihydrate ($CuCl_2{\cdot}2H_2O$, >98%), sodium citrate ($Na_3C_6H_5O_7{\cdot}2H_2O$, >99%), sodium borohydride ($NaBH_4$, >98%) and sodium hydroxide (NaOH, >96%) were obtained from Beijing Chemical Reagents Company and were used without any purification.

The Sn–Sb–Cu hollow nanospheres were prepared by reductive precipitation of the corresponding metal chlorides in $NaBH_4$ aqueous solution. In a typical synthesis, Solution 1 contained metal chlorides: $SnCl_2$ (0.08 M), $SbCl_3$ (0.03 M), $CuCl_2$ (0.06 M) and 1.0 M sodium citrate ($Na_3C_6H_5O_7{\cdot}2H_2O$) as a complexant. Solution 2 contained 0.5 M $NaBH_4$ as reducing agent and NaOH was added to adjust the pH of the solution to 12. The two separate aqueous solutions were cooled in iced water, respectively, and 20 ml Solution 1 was added drop-wise to 20 ml Solution 2 under strong magnetic stirring in 5 min. At the initial stage, the color of Solution 2 was turned into brown and then some small bubbles were observed and some black suspensions appeared with continued adding the solution containing metal ions. After completely adding Solution 1, the mixed solution was stirred for additional 1 h. During the whole process, the reaction vessel was cooled in the iced water. The resultant suspension was separated by centrifuge and rinsed several times using de-ionized water and acetone. Finally the precipitate was dried under vacuum at room temperature overnight.

The crystal structure of the product was characterized by X-ray powder diffraction (XRD) using an automated Rigaku X-ray diffractometer with monochromatic Cu Kα radiation. The morphology of the as-prepared samples was investigated by a Hitachi S-4800 field-emission scanning electron microscope (FE-SEM) at an accelerating voltage of 10 kV. Transmission electron microscopy (TEM) images were obtained on the Tecani F30 instrument at an accelerating voltage of 300 kV.

In order to measure the electrochemical performance, the electrodes were prepared by coating the slurry of the active material powders (80 wt.%), acetylene black (10 wt.%) and polyvinylidene fluoride (PVDF) (10 wt.%) dissolved in n-methyl pyrrolidinone on to a Cu foil substrate. After coating, the electrodes were pressed at 10 MPa and dried at 120 °C under vacuum for 24 h. Li metal foil was utilized as the counter electrode, 1 M $LiPF_6$ in ethylene carbonate (EC) and dimethyl carbonate (DMC) (1:1 by volume) was used as the electrolyte, and Celgard 2400 was used as the separator. Half-cells were assembled in an argon-filled glove-box. The cell performance was estimated galvanostatically at a current density of 100 mA g^{-1} for both charge (Li extraction) and discharge (Li insertion) at room temperature. The cells were cycled in the voltage range of 0.005–1.5 V (versus Li/Li^+). Cyclic voltammetric measurements were performed to examine the cathode and anode reaction using the above-mentioned cell in the voltage range of 2.5–0 V (versus Li/Li^+) at a sweep rate of 0.1 mV s^{-1}. Electrochemical impedance spectroscopy measurements were performed under open circle potential in an alternating current frequency range from 10000 to 0.01 Hz with an excitation signal of 5 mV.

3. Results and discussion

Fig. 1a shows the XRD patterns of the as-prepared Sn–Sb–Cu alloy powders after the co-reduction treatment. Not any ternary

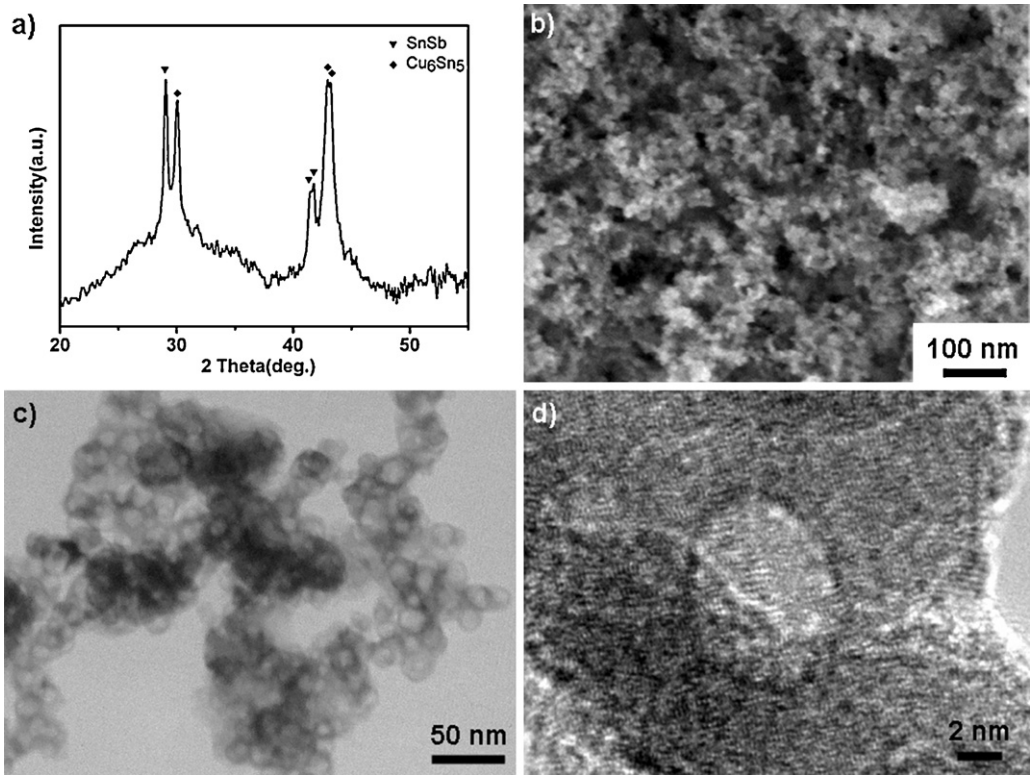

Fig. 1. (a) The XRD pattern taken from the as-synthesized Sn–Sb–Cu product. (b) FE-SEM image and (c and d) TEM images of the Sn–Sb–Cu hollow nanospheres.

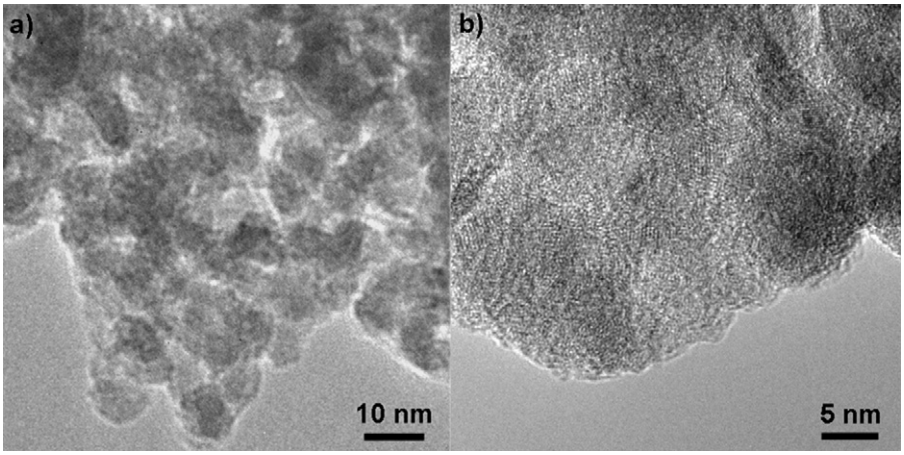

Fig. 2. TEM images of the Sn–Sb–Cu nanoparticles.

phase is observed in the XRD patterns, only the SnSb (JCPDS 33-0118) and Cu_6Sn_5 (JCPDS 45-1488) phases coexist in the Sn–Sb–Cu alloy composites. When Solution 1 contains 0.08 M $SnCl_2$, 0.03 M $SbCl_3$, 0.06 M $CuCl_2$ and 1.0 M sodium citrate, Sn–Sb–Cu hollow nanospheres are obtained. From the SEM image shown in Fig. 1b, it is apparent that the size the hollow spheres has a uniform distribution and is estimated to be about 15 nm. The TEM image (Fig. 1c) reveals that the product consists of spherical hollow particles. The structural details are investigated in a high-magnification TEM image (Fig. 1d), revealing that the Sn–Sb–Cu hollow spheres have a shell thickness of about 5 nm. Interestingly, it was found that the concentration of Solution 1 has a dramatic effect on the morphology of the product in the co-reduction reaction. When Solution 1 contains only 0.04 M $SnCl_2$, 0.015 M $SbCl_3$, 0.03 M $CuCl_2$ and 0.5 M sodium citrate, no hollow structures but only nanoparticles can be found. When Solution 1 was added to Solution 2, H_2 bubbles can hardly be observed in the reaction system. Solution 2 was turned into brown, but no black suspensions appeared even if Solution 1 was completely added. The black suspensions were observed after additional 1 h stirring process. However, Fig. 2 shows the TEM images of the Sn–Sb–Cu nanoparticles, which reveal that the particle size of the nanoparticles is less than 10 nm, smaller than the hollow nanospheres.

As not any hard templates or surfactants were added in the system, a bubble assisted formation mechanism is proposed, as illustrated in Fig. 3. During the formation process, H_2 bubbles which are generated *in situ* on combination with alloy nuclei play a significant role in the formation of the hollow nanospheres. The alloy hollow nanospheres are formed by reduction, nucleation and growth in the dispersive system. At the initial stage of the reaction, the alloy nuclei in combination with H_2 bubbles are generated through the reduction of metal ions. In the case of hollow nanospheres, large amount of H_2 are produced during reaction. Small size H_2 bubbles coagulate in the dispersion system to form bigger H_2 bubbles which provide the spherical template [26]. The majorities of alloy nuclei are absorbed on the surface of the bigger H_2 bubbles, and lead to the formation of hollow nanospheres (Fig. 3b). Altering the concentration of Solution 1 will easily tune the morphologies of Sn–Sb–Cu alloy composites nanostructures from hollow nanospheres to nanoparticles. A possible reason is that lower concentrations of metal ions slow down the releasing rate of H_2 gas, and the size of H_2 bubbles has significantly decreased. The small H_2 bubbles result in the bigger surface tension between the solid–gas interface and counterworking the absorption of the alloy nuclei on the surface of H_2 bubbles. Therefore, the alloy nuclei are prior to congregate with each other but not to deposit on the surface of H_2 bubbles, leading to the formation of nanoparticles (Fig. 3a).

The discharge/charge curves of the Sn–Sb–Cu hollow nanospheres for the first, fifth, tenth and twentieth cycles are shown in Fig. 4a. The slopes above 0.8 V at the first discharge are observed for all the three samples, which correspond to the formation of the SEI (solid electrolyte interphase) layer and irreversible reduction of surface impurities such as oxides and hydroxides [27]. The existence of the impurities also contributes to large irreversible capacities during the first cycle. The voltage region between 0.8 V and 0.7 V is related to the reaction of Li–Sb alloy reactions, Li inserts SnSb to form Li_3Sb and Sn [28]. The voltage region below 0.7 V is attributed to the multi-step Li–Sn alloy reactions. The corresponding regions in the charge curves which are attributed to the delithiation reaction can also be observed, respec-

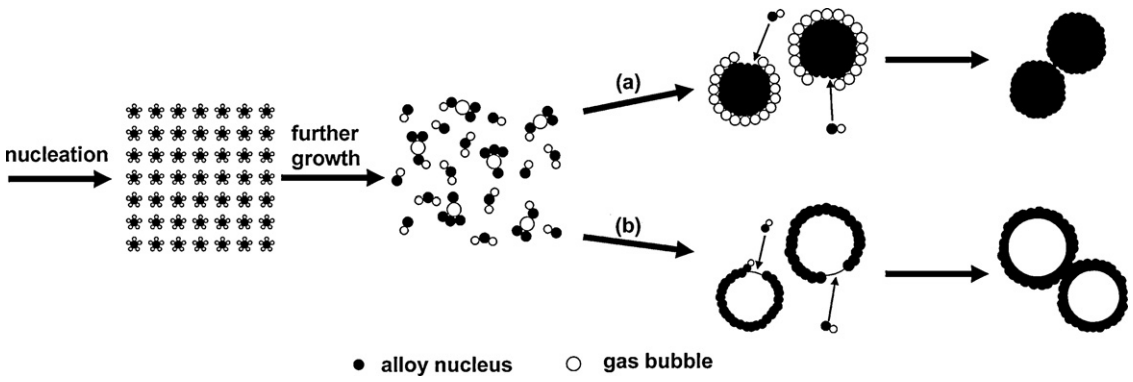

Fig. 3. Schematic illustration of the experimental procedure that generates Sn–Sb–Cu (a) nanoparticles and (b) hollow nanospheres.

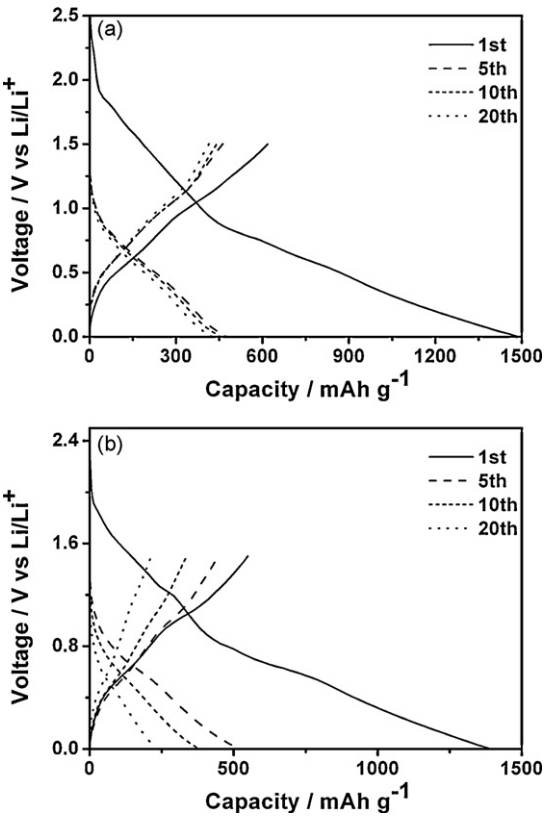

Fig. 4. The discharge/charge curves of the Sn–Sb–Cu (a) hollow nanospheres and (b) nanoparticles.

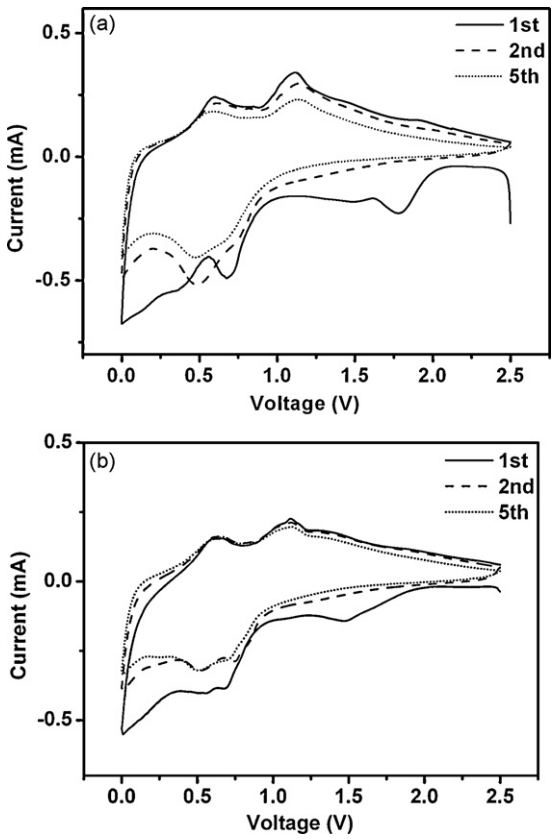

Fig. 5. Cyclic voltammogram of the Sn–Sb–Cu (a) hollow nanospheres and (b) nanoparticles.

tively. The discharge/charge curves of the Sn–Sb–Cu nanoparticles shown in Fig. 4b are similar to that of the hollow spheres. Because both hollow spheres and nanoparticles have the same elemental compositions and alloy phases. Although the two products have different morphology, this does not affect the occurrence of the electrochemical reactions. Concerning about the capacity change, the capacity of the Sn–Sb–Cu hollow nanospheres reaches almost the same values after the first charge–discharge cycle, but the capacity of the nanoparticles has a rapid degradation. This result suggests that the hollow nanospheres have good capacity retention during the discharge/charge process compared with the nanoparticles.

The electrode reaction processes of the as-prepared Sn–Sb–Cu samples are distinguished more clearly from the cyclic voltammogram. The cyclic voltammograms of the Sn–Sb–Cu hollow nanospheres and nanoparticles are shown in Fig. 5a and b, respectively. Owning to the same electrochemical reaction, all the peaks appear at the same voltage value for both two products. An additional reduction peak at the potential about 1.7 V (versus Li/Li^+) is observed during the first cycle, and no longer appeared in the later cycles, which is attributed to the irreversible reduction of surface impurities. The broad peak between 1.2 and 1.6 V corresponds to the formation of SEI films [27], which is always observed during the initial discharge process. The two peaks below 1.0 V are associated with the Li–Sb and Li–Sn alloying process, respectively, which demonstrates that Li insertion reactions act in a step-wise process [28]. The corresponding oxidation peaks also prove that the Li extraction act in a similar process. Although the two products have the same composition, there are still some differences for the two products in the cyclic voltammogram. It is observed that the peaks of the Sn–Sb–Cu nanoparticles have significantly broadened compared with that of the hollow spheres. This can be attributed to the kinetic factors of the electrochemical reaction. The specific hollow nanostructures can provide shorter diffusion length for ionic and electronic transport, so that the kinetics of the electrochemical reaction is improved. This means the hollow nanospheres will react more efficient at the same current density compared with the nanoparticles.

Electrical conduction and ion transfer were investigated by electrochemical impedance spectroscopy (EIS). Fig. 6 shows the complex plane plots of the impedance of the two Sn–Sb–Cu products before discharge/charge processes (at open circuit potential). The complex plane plots for each sample can be divided into high frequency semicircle and low frequency sloping line. A typical EIS of lithium cell can be fitted by the equivalent circuit shown in inset of Fig. 6. The Rb is bulk resistance of the cell, which reflects electrical conductivity of electrodes, electrolyte and separator; R_{sei} and C_{sei} are resistance and capacitance of the solid state interface

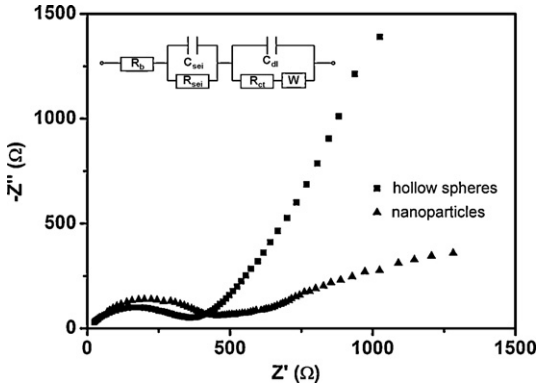

Fig. 6. Complex plane impedance plots of the Sn–Sb–Cu samples at AC voltage amplitude of 5 mV. The *inset* is the equivalent circle.

layer formed on the surface of electrode, which can be neglected in our experimental test, as the SEI layers do not form before discharge/charge processes; R_{ct} and C_{dl} are faradic charge-transfer resistance and its relative double layer capacitance, which correspond to the semicircle at high frequencies; W is the Warburg impedance related to a combination of the diffusion effects of lithium-ion on the interface between the active material and electrode, which is generally indicated by the straight sloping line at low frequency end. The combination of R_{ct} and W is called faradic impedance, which reflects kinetics of the electrochemical reaction. Low R_{ct} generally corresponds to a fast kinetics of faradic reaction, and there is a close correlation between the R_{ct} and the apparent diffusivity of Li ions in the electrode [29]. It is clear that R_{ct} of the hollow sphere sample is smaller than that of the nanoparticle sample. This can be attributed to the difference of their nanostructures. The specific hollow structure can increase the exchange rate of electrode material and electrolyte ions. Furthermore, in the low frequency area, the phase angle for impedance plot of the hollow sphere sample is much higher than that of the nanoparticle sample, indicating that the hollow nanostructure can enhance the diffusivity of electrolyte ions in the electrode material [30]. These results prove that the specific hollow nanostructure can significantly improve the kinetics of the electrochemical reactions.

Fig. 7a compares the discharge capacities of the Sn–Sb–Cu hollow nanospheres and that of the Sn–Sb–Cu nanoparticles under the same condition. The discharge capacities of the Sn–Sb–Cu nanoparticles show significant fading during cycling, since the discharge/charge process is accompanied by severe volume change. However, except the first cycles, Sn–Sb–Cu hollow nanospheres exhibit good cycling abilities and high reversible specific capacities, which still show 390 mAh g^{-1} reversible capacities after 30 cycles, much higher than the Sn–Sb–Cu nanoparticles (180 mAh g^{-1}), The average capacity fading of the sample is estimated to be 0.60% per cycle after the second cycle, which is much smaller than that of the Sn–Sb–Cu nanoparticles, 2.5%. The reversible capacities of the Sn–Sb–Cu hollow nanospheres are also larger than the theoretical capacities of the commercially used carbon-based anode materials (372 mAh g^{-1}). Concerning to the large density which metal alloys acquired, the hollow nanospheres obtained much larger volumetric capacities and power densities than the carbon-based anode materials. The result indicates the potential applications of the alloy hollow nanospheres as anode materials of lithium-ion batteries. Fig. 7b shows the columbic efficiency of the as-prepared samples. Both the Sn–Sb–Cu hollow nanospheres and Sn–Sb–Cu nanoparticles have evidently low columbic efficiency in the first cycle, which can be attributed to the SEI formation and irreversible reduction of oxide and hydroxylic impurities. In the following cycles, the Sn–Sb–Cu hollow nanostructures exhibit higher columbic efficiencies, which of above 95% are observed, much higher than that of the Sn–Sb–Cu nanoparticles. This would also be attributed to the good

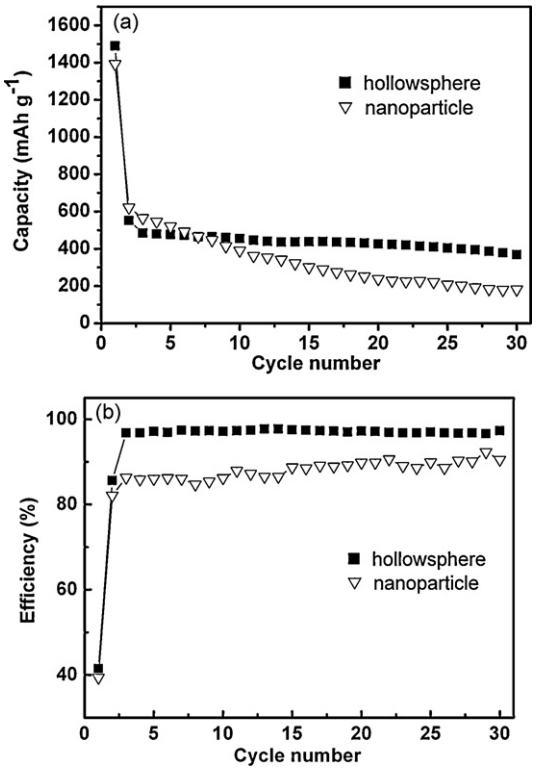

Fig. 7. (a) Discharge capacity and (b) electrode efficiency of the Sn–Sb–Cu hollow spheres and nanoparticle, respectively.

cycling performance of the Sn–Sb–Cu hollow nanospheres due to the buffer effects of the hollow structure.

The TEM images of the Sn–Sb–Cu hollow nanostructures after 30 cycles are shown in Fig. 8. According to the TEM images, there are still some regions that contain amorphous materials. This is due to the existence of polymer binder and carbon black which cannot be completely removed from the product. It is observed that the diameters of the alloy particles are still less than 20 nm, indicating the prevention of aggregation between the active materials, but the nanostructures are not completely preserved. The hollow structure cannot be observed in many alloy particles, only a part of the particles still have the hollow structures. Although these particles still have a hollow structure, the shell thicknesses have significantly increased. This can be attributed to the volume change in the cycling process. During the discharge process, large volume expansion occurs and the active materials move towards the center of the particles, but these materials cannot totally move back. As a result, the shell thicknesses of the hollow spheres have increased a lot after 30 cycles of discharge/charge processes, and some of the

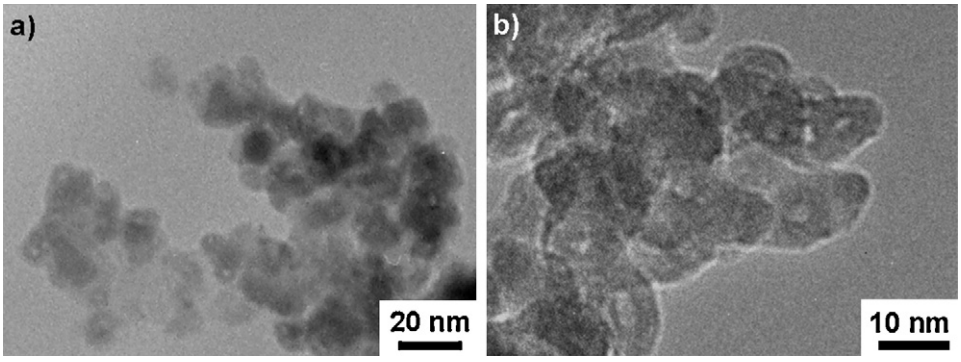

Fig. 8. TEM images of the Sn–Sb–Cu hollow nanospheres after 30 cycles.

hollow spheres have lost their original hollow structures. Due to this effect, the volume expansion outside the particles has been alleviated, and the aggregation between the active materials has been prevented.

The improved reversible capacity and good cyclic ability up to 30 cycles of the Sn–Sb–Cu hollow nanospheres can be attributed to the specific nanostructure. The Sn–Sb–Cu hollow nanospheres can enhance the electrochemical properties in the following ways. First, as a result of small shell thickness of the hollow nanospheres, the mass and charge find shorter diffusion lengths for ionic and electronic transport and the effective electrode/electrolyte contact area is enhanced [31], so that the kinetics of the electrochemical reaction are improved. Second, the Sn–Sb–Cu hollow nanospheres have a specific loose structure, which sufficiently alleviate the mechanical stress caused by the severe volume change during lithium insertion and extraction, so that the aggregation between the active materials is prevented. According to the above results, the prepared Sn–Sb–Cu hollow nanospheres possess superior lithium storage capacity when used as an anode material in lithium-ion battery. In agreement with the previous reports [32–35], it seems that nanomaterials with hollow structure can manifest large improvements in electrochemical performance for lithium-ion batteries.

4. Conclusions

In summary, the Sn–Sb–Cu hollow nanospheres have been successfully prepared by co-reducing the metal chloride in alkaline solution. The concentration of metallic salt is of great importance for preparing the specific hollow nanostructures. Compared with the alloy nanoparticles, the hollow nanospheres exhibit improved electrochemical properties when used as anode materials for lithium-ion batteries. The hollow nanospheres improve the kinetics of the electrochemical reaction by providing large electrode/electrolyte contact area and fast diffusion rate for ions and electrons. The good cyclic retention of the Sn–Sb–Cu hollow nanospheres is mainly attributed to the specific loose structures, which provide large interspace to alleviate the severe volume expansion caused by the lithium insertion during discharge process. The improved electrochemical properties of the Sn–Sb–Cu hollow nanospheres indicate that the suitable morphological modification would be an efficient strategy to improve the electrochemical properties of metal-based anode materials for lithium-ion batteries. The bubble assisted synthesis method reported here can be readily explored for fabricating hollow nanostructures of other alloy system for functional material applications.

Acknowledgments

This work was supported by the National Natural Science Funds of China (Nos. 20971009 and 20821091), the Ministry of Science and Technology of the People's Republic of China (Nos. 2009CB939902 and 2010CB631301), the Ministry of Education of the People's Republic of China (No. 707002) and Delta Electronics INC.

References

[1] M. Yang, J. Ma, C.L. Zhang, Z.Z. Yang, Y.F. Lu, Angew. Chem. Int. Ed. 44 (2005) 6727.
[2] S.W. Kim, M. Kim, W.Y. Lee, T. Hyeon, J. Am. Chem. Soc. 124 (2002) 7642.
[3] J. Gao, B. Zhang, X. Zhang, B. Xu, Angew. Chem. Int. Ed. 45 (2006) 1220.
[4] C.I. Zoldesi, A. Imhof, Adv. Mater. 17 (2005) 924.
[5] S. Han, B. Jang, T. Kim, S.M. Oh, T. Hyeon, Adv. Funct. Mater. 15 (2005) 1845.
[6] Y. Vasquez, A.K. Sra, R.E. Schaak, J. Am. Chem. Soc. 127 (2005) 12504.
[7] A.E. Berkowitz, H. Harper, D.J. Smith, H. Hu, Q. Jiang, V.C. Solomon, H.B. Radousky, Appl. Phys. Lett. 85 (2004) 940.
[8] D.B. Wang, C.X. Song, Z.S. Hu, X. Fu, J. Phys. Chem. B 109 (2005) 1125.
[9] J.M. Bai, J.P. Wang, Appl. Phys. Lett. 87 (2005).
[10] Q. Peng, Y.J. Dong, Y.D. Li, Angew. Chem. Int. Ed. 42 (2003) 3027.
[11] G. Tong, J. Guan, Z. Xiao, F. Mou, W. Wang, G. Yan, Chem. Mater. 20 (2008) 3535.
[12] Y. Idota, T. Kubota, A. Matsufuji, Y. Maekawa, T. Miyasaka, Science 276 (1997) 1395.
[13] H. Bryngelsson, J. Eskhult, L. Nyholm, M. Herranen, O. Alm, K. Edstrom, Chem. Mater. 19 (2007) 1170.
[14] C. Kim, M. Noh, M. Choi, J. Cho, B. Park, Chem. Mater. 17 (2005) 3297.
[15] Y. Wang, F. Su, J.Y. Lee, X.S. Zhao, Chem. Mater. 18 (2006) 1347.
[16] M. Winter, J.O. Besenhard, M.E. Spahr, P. Novak, Adv. Mater. 10 (1998) 725.
[17] J. Yang, M. Winter, J.O. Besenhard, Solid State Ionics 90 (1996) 281.
[18] J. Yang, Y. Takeda, N. Imanishi, O. Yamamoto, J. Electrochem. Soc. 146 (1999) 4009.
[19] F.S. Ke, L. Huang, H.B. Wei, J.S. Cai, X.Y. Fan, F.Z. Yang, S.G. Sun, J. Power Sources 170 (2007) 450.
[20] H. Kim, J. Cho, Electrochim. Acta 52 (2007) 4197.
[21] J. Xie, X.B. Zhao, G.S. Cao, J.P. Tu, J. Power Sources 164 (2007) 386.
[22] H. Guo, H. Zhao, X. Jia, X. Li, W. Qiu, Electrochim. Acta 52 (2007) 4853.
[23] D.G. Kim, H. Kim, H.J. Sohn, T. Kang, J. Power Sources 104 (2002) 221.
[24] J. Hassoun, S. Panero, P. Simon, P.L. Taberna, B. Scrosati, Adv. Mater. 19 (2007) 1632.
[25] H. Guo, H. Zhao, X. Jia, Electrochem. Commun. 9 (2007) 2207.
[26] S.M. Yoon, H.C. Choi, Curr. Appl. Phys. 6 (2006) 747.
[27] M. Wachtler, J.O. Besenhard, M. Winter, J. Power Sources 94 (2001) 189.
[28] M. Winter, J.O. Besenhard, Electrochim. Acta 45 (1999) 31.
[29] S.S. Zhang, K. Xu, T.R. Jow, Electrochim. Acta 49 (2004) 1057.
[30] M.W. Xu, D.D. Zhao, S.J. Bao, H.L. Li, J. Solid State Electrochem. 11 (2007) 1101.
[31] A.S. Arico, P. Bruce, B. Scrosati, J.M. Tarascon, W. Van Schalkwijk, Nat. Mater. 4 (2005) 366.
[32] X.W. Lou, Y. Wang, C. Yuan, J.Y. Lee, L.A. Archer, Adv. Mater. 18 (2006) 2325.
[33] Q. Zhao, Y. Xie, T. Dong, Z. Zhang, J. Phys. Chem. C 111 (2007) 11598.
[34] N. Du, H. Zhang, J. Chen, J.Y. Sun, B.D. Chen, D.R. Yang, J. Phys. Chem. B 112 (2008) 14836.
[35] H. Kim, J. Cho, Chem. Mater. 20 (2008) 1679.